This article has been accepted for publication in a future issue of this journal, but has not been fully edited. Content may change prior to final publication. Citation information: DOI 10.1109/TVT.2018.2878352, IEEE Transactions on Vehicular Technology

Estimation of the K-factor for Temporal Fading from Single-Snapshot Wideband Measurements

Pan Tang, *Student Member, IEEE,* Jianhua Zhang, *Senior Member, IEEE,* Andreas F. Molisch, *Fellow, IEEE,* Peter J. Smith, *Fellow, IEEE,* Mansoor Shafi, *Life Fellow, IEEE,* Lei Tian, *Member, IEEE,*

***Abstract*—The Ricean K-factor is the ratio of the power of the deterministic multipath component (MPC) and the power of all other stochastic MPCs. The classical moment-based method has been successfully used to estimate the K-factor from time series measurements. In this paper, we apply this method to estimate the K-factor for narrowband temporal selectivity, based upon the analysis of frequency-selectivity in single-snapshot wideband measurements. We also derive the theoretical bias of this estimator and find it depends jointly on the number of channel transfer function envelope samples across the measurement bandwidth, the correlation among such samples, and the K-factor values. Qualitative analysis indicates that the bias increases nearly linearly with the K-factor ($K \geq 1$ on the linear scale) and is affected by correlation amongst the samples. Furthermore, the bias is inversely proportional to the number of samples. Simulations confirm the validity of the derivations. Moreover, a measurement campaign is designed at 28 GHz with a system bandwidth of 400 MHz in an urban micro-cell scenario. The proposed estimator is used to extract the statistics of the K-factor in line of sight and non-line of sight scenarios. The relationship between the K-factor and distance is investigated and a linear model is used to characterize it.**

***Index Terms*—K-factor, wideband channel, estimation, bias, millimeter wave.**

I. Introduction

In wireless communication environments, different multipath components (MPCs) arising from reflection, diffraction and scattering processes, impinge on the receiver. Each MPC has a different magnitude, phase, and angle of arrival. The wireless channel gain is an important quantity and is commonly assumed to be a complex Gaussian random variable, by invoking the central limit theorem [1]. Under the Gaussian assumption, if there is a deterministic[1] component in the channel, the complex channel gain is nonzero-mean complex Gaussian, and the envelope follows a Ricean probability density function (PDF). Note that for a mobile channel, the non-zero mean is not apparent until the deterministic phase evolution is tracked. The Ricean factor, also named *K-factor*, is the power ratio of the deterministic component to that of the other, stochastic, components.

The K-factor can be a measure of small scale variations in time, space, or frequency, i.e., temporal, spatial or spectral selectivity. The smaller the K-factor, the more severe the selectivity, with the limiting case of $K = 0$ corresponding to Rayleigh fading [2] [3]. Knowledge of K-factor statistics is important for the design and performance analysis of wireless systems. Furthermore, some link-adaptive technologies are analyzed and optimized for Ricean fading [4] [5] [6] and in [7] [8] [9], the capacity analysis of a wireless communication system depends on the K-factor. These examples show that estimation of the K-factor is of significant importance for the establishment of reliable and representative channel models.

A. Literature review

In the existing literature, several different estimators have been proposed. The maximum-likelihood (ML) estimator [10] and the method of moments [11] were introduced to calculate the K-factor using samples of the received signal envelope. The ML estimator in [12] employs the in-phase and quadrature-phase (IQ) samples, and thus has superior bias and efficiency for short data records. However, it is more complex and its performance depends on good initial values. In [13], a Bayesian approach was used to overcome the drawbacks of the ML estimator.

All the above estimators assume that the channel is narrowband and time-varying. However, most current wireless systems are wideband. For example, in millimeter wave mobile communication systems, over 1 GHz of bandwidth may be used [14], while multipaths with delays of several hundred nanoseconds or even microseconds are present. The distribution of the envelope of a wideband signal that varies in time was studied in [15]. On the other hand, most of the measurements in millimeter wave bands are conducted when the measurement system is static due to the typical constraints of the measurement platforms [16] [17]. Also, most measurements are designed such that the environment can also be considered to be static. Thus K-factor estimators for such fixed-location measurements are required. In [18], a K-factor estimator for a multiple-input-multiple-output multipath

Pan Tang, Jianhua Zhang and Lei Tian are with State Key Lab of Networking and Switching Technology, Beijing University of Posts and Telecommunications, Beijing, 100876, China (email: {tangpan27, jhzhang, tianlbupt}@bupt.edu.cn).

Andreas F. Molisch is with the Ming Hsieh Department of Electrical Engineering, University of Southern California, Los Angeles, CA 90089 (email: molisch@usc.edu).

Peter J. Smith is with the School of Mathematics and Statistics, Victoria University of Wellington, Wellington 6140, New Zealand (email: peter.smith@vuw.ac.nz).

Mansoor Shafi is with the Spark New Zealand, Wellington 6011, New Zealand (email: mansoor.shafi@spark.co.nz).

[1]The notation of deterministic and stochastic component follows the classical paper by Rice. In wireless communications, MPCs are not inherently deterministic or stochastic. In the literature, the "deterministic" component is usually set as the line-of-sight component, and the "stochastic" components are all other MPCs. However, this interpretation is not necessarily general, and can even be misleading, since, e.g., the K-factor can be nonzero even in the complete absence of a line-of-sight component.

This article has been accepted for publication in a future issue of this journal, but has not been fully edited. Content may change prior to final publication. Citation information: DOI 10.1109/TVT.2018.2878352, IEEE Transactions on Vehicular Technology

channel was proposed, which computed the K-factor as the ratio of the power in the first delay bin divided by the power in the other delay bins. However this is not accurate if there are stochastic components in the first delay bin. Besides, if the deterministic component is a reflected component, it is perhaps not in the first delay bin. In [19] and [20], the traditional moment method was used to calculate the K-factor on each delay bin or carrier frequency separately. The calculated K-factor is not the traditional Ricean factor that we are interested in because each bin can contain contributions from only one or several MPCs rather than all MPCs in the channel. In the more recent literature, [21] computed the empirical distribution of the small-scale temporal selectivity values of all resolvable paths and compared the result with the Ricean distribution to obtain the K-factor of a millimeter wave channel in an indoor scenario. In [22], measurements of the small-scale spatial fading of the received signal voltage amplitude were used to find various spatial selectivity distributions at 73 GHz. Ray tracing was also used to extract the wideband K-factor at 28 GHz in urban street-canyon environments [23], but estimators suitable for ray tracing where the deterministic component can be perfectly isolated are not necessarily suitable for measurement analysis.

Another important aspect of K-factor estimators is the bias and variance for a finite number of samples. In [24], Monte Carlo simulations were used to ascertain the minimum number of samples required to estimate the K-factor within a specified confidence interval. It was found that the minimum number of samples depended upon the value of the K-factor, the correlation between successive samples and the sample interval. The impact of the correlation on the performance of the K-factor estimators was analyzed in [25]. However, these analyses are mostly based on simulations without theoretic derivations.

B. Contributions of this paper

In this paper, we propose a method of estimating the K-factor for narrowband temporal selectivity based on analyzing spectral selectivity. Importantly, this method does not require multiple spatial samples, i.e., we can obtain the K-factor based on a single (static) measurement. Furthermore, we derive the bias of this estimator, which agrees well with simulations. We find that the bias depends jointly on the number of channel transfer function envelope samples across the measurement bandwidth, the correlation between successive samples, and the K-factor values. Finally, we use this estimator to extract the statistics of the K-factor of a millimeter wave channel in an urban micro-cell scenario from measured data. These results can be helpful for designing mobile wireless communication systems.

The contributions of this paper are as follows:

- We propose a method of estimating the K-factor for narrowband temporal selectivity based on analyzing the spectral selectivity.
- We derive the bias of the estimator both for frequency-based and time-based K-factor estimators.
- We show, via derivation and simulation, that the bias of the estimator increases nearly linearly with the K-factor values ($K \geq 1$ on the linear scale) while the bias is inversely proportional to the number of samples. Also, we show that when there is strong correlation between successive samples, the correlation has a major influence on bias.
- We show, via analyzing measurement data, the statistics of the K-factor in an urban microcell scenario. In addition, we investigate the relationship between the K-factor and the measured distance for both the line of sight (LOS) and non-line of sight (NLOS) scenarios.

C. Paper organization

The rest of this paper is organized as follows. Section II introduces the K-factor estimator. The theoretical derivations of the bias of this estimator are presented in Section III. Corresponding numerical results based on simulations are given in Section IV. Section V describes the measurement setup and scenarios. The statistics of the millimeter wave channel K-factor in an urban micro-cell scenario are analyzed in Section VI and VII. Finally, Section VIII concludes this paper.

II. The K-factor Estimator

A frequency-flat, time-varying channel impulse response (CIR) with a deterministic component can be expressed as [11]

$$h(t) = V_D + \sqrt{P_R} g(t), \tag{1}$$

where V_D is a complex constant, which indicates the deterministic component with a power gain of P_D, $\sqrt{P_R} g(t)$ is a complex, zero-mean Gaussian process which represents the stochastic (typically reflected, diffracted, or diffusely scattered) components with the average power gain of $2P_R$. The envelope of $h(t)$ can be described by a Ricean PDF, which is

$$f_{\text{Ricean}}(x) = \frac{x}{P_R} \exp\left(-\frac{x^2 + P_D}{2P_R}\right) \mathrm{I}_0\left(\frac{x\sqrt{P_D}}{P_R}\right),$$

where I_0 is the zero-th order modified Bessel function of the first kind. Hence, the K-factor is

$$K = \frac{P_D}{2P_R}. \tag{2}$$

According to [11], the K-factor can be calculated by computing the moments of the envelope of $h(t)$.

A wideband receiver can resolve MPCs according to their delay; the resolution can be approximated by a "delay bin", whose duration is the inverse of the measurement bandwidth. Hence, the CIR can be defined as[2]

$$h(t;\tau) = V_D \delta(\tau - \tau_0) + \sum_{m=1}^{M} \sqrt{P_m} g_m(t) \delta(\tau - \tau_m), \tag{3}$$

where $\sqrt{P_m} g_m(t)$ represents the sum of MPCs with the excess delay of τ_m, $2P_m$ is the power gain, M is the number of delay bins, V_D represents the deterministic component in the delay

[2]The following channel response equations are well known, for more details see, e.g., [1].

This article has been accepted for publication in a future issue of this journal, but has not been fully edited. Content may change prior to final publication. Citation information: DOI 10.1109/TVT.2018.2878352, IEEE Transactions on Vehicular Technology

bin τ_0 and $\delta(\cdot)$ is the Dirac function. It is noteworthy that τ_0 may not be the first delay bin because the deterministic component could be a reflected component. In the frequency domain, samples across the channel's bandwidth can be considered to be different narrowband channel realizations. In measured results, such samples can easily be taken to be the different samples taken during a single sweep, if a vector network analyzer is used for the measurements. Alternately, they can be different samples in frequency resulting from the Fourier transform of a CIR measured with a time-domain channel sounder, e.g., a correlative sounder. They have regular spacing and are of a similar nature to orthogonal frequency division multiplexing subcarriers; note, though, that the channel sounding and description is independent of any communications system for which the channel modeling is done. It is herein conjectured, and demonstrated, that the K-factor that would characterize narrowband temporal fading on the measured channel can be estimated by analyzing the transfer function estimate (TFE) $H(t;f)$, under certain conditions. The TFE can be expressed as

$$H(t;f)=\int_{\tau} h(t;\tau)\exp(-j_c 2\pi f\tau)d\tau. \tag{4}$$

where j_c is equal to $\sqrt{-1}$, i.e., the imaginary unit.

Assuming there are n narrowband spectral samples, we can get

$$H_i = V_D\exp(-j_c 2\pi f\tau_0)+\sqrt{P_R}g_i^{'},\ i=1,2...,n, \tag{5}$$

where H_i is the TFE, $H(t;i\Delta f)$, on the ith spectral sample, $P_R=\sum_{m=1}^{M}P_m$ and $g_i^{'}$ is a complex zero-mean Gaussian process. The reader should note that the complex Gaussian condition can be satisfied using the central limit theorem only if a sufficient number (usually about 10) of MPCs are received. The Ricean factor extraction should only be applied, therefore, if it can be shown to be reasonable that the central limit theorem holds and the Gaussian model applies.[3] Using (2), H_i can be normalized as

$$H_i=\sqrt{\frac{K}{K+1}}\exp(-j_c 2\pi f\tau_0)+\sqrt{\frac{1}{K+1}}g_i^{'},\ i=1,2...,n. \tag{6}$$

In wideband systems, the impact of multipath propagation results in spectral selectivity of the channel [1] [27]. Furthermore, the different spectral samples are correlated with each other if they are sufficiently closely spaced,[4] and such correlation can be accounted for by using the relationship

$$g_j^{'}=\rho_{i,j}g_i^{'}+\sqrt{1-|\rho_{i,j}|^2}e_i,\ j=1,2...,n, \tag{7}$$

where e_i and $g_i^{'}$ are independent $CN(0,1)$ (complex normal) variables, and e_i can be considered as a noise variable. $\rho_{i,j}$ is the correlation coefficient between the $i-th$ and $j-th$ spectral samples. Based on the above mathematical descriptions, we use the moment method [11] to estimate the K-factor as follows

$$G_a=\frac{1}{n}\sum_{i=1}^{n}|H_i|^2, \tag{8}$$

$$G_v=\frac{1}{n-1}\left(\sum_{i=1}^{n}|H_i|^4-nG_a^2\right), \tag{9}$$

$$\hat{K}=\frac{\sqrt{G_a^2-G_v}}{G_a-\sqrt{G_a^2-G_v}}, \tag{10}$$

where G_a and G_v denote the first and second sample moments separately and $\hat{K}$ is the estimated K-factor. We note that equations (1)-(7) are generally valid for Ricean fading, and we could estimate the Ricean factor by any estimator mentioned in Section I-A. However, the bias analysis in Section III is specific to the moment method estimator.

To further demonstrate the availability of the proposed method, we compare it with the typical K-factor estimation method, in which we use the moments of a time series of amplitudes of CIRs to estimate the K-factor. If wide-sense stationary uncorrelated scattering (WSSUS) holds, the wideband channel CIR within a small time segment can be written as

$$h(t,\tau)=V_D\delta(\tau-\tau_0)+\sum_{m=1}^{M}a_m e^{j_c 2\pi f_{\max}\cos(\vartheta_m)t+\theta_m}\delta(\tau-\tau_m), \tag{11}$$

where a_m is the random amplitude, $f_{\max}$ is the maximum Doppler frequency, ϑ_m is the arrival angle, θ_n is the random phase. This equation is valid, by definition, within the "region of stationarity". Note that in the experiments in the later sections of this paper, we conservatively choose an area with a diameter of 10λ as a WSS interval when analyzing the time-series measurements. In the typical method, we firstly sum up CIRs in the delay domain as follows (i.e., generating a time-variant signal that is narrowband, as summation in the delay domain is equivalent to low-pass filtering)

$$h(t)=\sum_{m=0}^{M}h(t,\tau_m)=V_D+\sum_{m=1}^{M}a_m e^{j_c 2\pi f_{\max}\cos(\vartheta_m)t+\theta_m}. \tag{12}$$

If the number of MPCs, M, is big enough, then, according to the central limit theorem, we can get $\sum_{m=1}^{M}a_m e^{j_c 2\pi f_{\max}\cos(\vartheta_m)t+\theta_m}\sim CN(0,\sum_{m=1}^{M}|a_n|^2)$, $h(t)\sim CN(V_D,\sum_{m=1}^{M}|a_n|^2)$ and samples of $h(t)$, $h(t_i)$, are measured in the ith different space/time position, $i=1,2,...,I$. Then, we can use the moment method to calculate the K-factor as follows, where "nb" is the abbreviation of "narrowband" and indicates the typical

[3]This can be accomplished by verifying that there are more than 10 delay bins in the CIR estimate where significant power is received, or if there are fewer than 10, using spectral smoothing and forward-backward averaging, followed by an eigenvalue decomposition of the correlation matrix for the frequency-domain samples, and application of the Akaike information criterion or minimum description length information theory criteria to estimate the number of MPCs received. A cursory check might also be conducted by using the Kolmogorov Smirnoff (KS) test or the Chi-square test to assess whether the cumulative distribution function (CDF) or the PDF of the complex frequency-domain samples can be modelled using a Gaussian CDF or PDF [26].

[4]We henceforth assume that the channel is measured on discrete spectral samples, which is in line with both multicarrier communication systems and vector network analyzers, which are frequently used for channel sounding.

This article has been accepted for publication in a future issue of this journal, but has not been fully edited. Content may change prior to final publication. Citation information: DOI 10.1109/TVT.2018.2878352, IEEE Transactions on Vehicular Technology

method,

$$G_{a-\mathrm{nb}} = \frac{1}{I}\sum_{i=1}^{I}|h(t_i)|^2, \tag{13}$$

$$G_{v-\mathrm{nb}} = \frac{1}{I-1}\left(\sum_{i=1}^{I}|h(t_i)|^4 - IG_{a-\mathrm{nb}}^2\right), \tag{14}$$

$$\hat{K}_{-\mathrm{nb}} = \frac{\sqrt{G_{a-\mathrm{nb}}^2 - G_{v-\mathrm{nb}}}}{G_{a-\mathrm{nb}} - \sqrt{G_{a-\mathrm{nb}}^2 - G_{v-\mathrm{nb}}}}. \tag{15}$$

Here, the true K-factor can be expressed as

$$K = \frac{|V_D|^2}{\sum_{m=1}^{M}|a_m|^2}. \tag{16}$$

For the proposed method, we first get the transfer function as follows,

$$H(t,f) = V_D e^{-j_c 2\pi f\tau_0} + \sum_{m=1}^{M} a_m e^{j_c(2\pi f_{\max}\cos(\vartheta_m)t + \theta_m - 2\pi f\tau_m)}. \tag{17}$$

$H(0, f_j)$ is the channel transfer function in the jth frequency position for a single snapshot. Then, we use the moment-method to calculate the K-factor in the frequency domain using equations (8)-(10). Here, the true K-factor can be expressed as

$$K = \frac{|Ve^{-j_c 2\pi f\tau_0}|^2}{\sum_{m=1}^{M}|a_m|^2} = \frac{|V_D|^2}{\sum_{m=1}^{M}|a_m|^2}. \tag{18}$$

Comparing (16) with (18), we observe that both methods are correctly estimating the same K-factor under the condition of WSSUS. An analysis of measured time series data is given in Section VI by using these two methods.

III. The Derivation of the Bias

A. The Mathematical Derivation

Before deriving the bias of this estimator, it is required to estimate the mean and variance of G_a and G_v respectively, which are the main components of this estimator. As shown in Appendix A,

$$\begin{aligned}&\mathrm{E}(G_a) = 1,\ \mathrm{Var}(G_a) = \frac{2K+1}{n(K+1)^2} + \left(1-\frac{1}{n}\right)\Delta,\\ &\mathrm{E}(G_v) = \frac{2K+1}{(K+1)^2} - \Delta,\ \mathrm{Var}(G_v) = \frac{8K^2+32K+8}{n(K+1)^4} + \Delta',\end{aligned} \tag{19}$$

where Δ, Δ' are related to the K-factor and the correlation coefficients as follows

$$\Delta = \frac{1}{n(n-1)}\sum_{i=1}^{n}\sum_{j\neq i,j=1}^{n}\frac{2K\mathrm{Re}(\rho_{i,j}) + |\rho_{i,j}|^2}{(K+1)^2}, \tag{20}$$

$$\begin{aligned}\Delta' =& \sum_{i=1}^{n}\sum_{j=1,j\neq i}^{n}\frac{4|\rho_{i,j}|^4 + 16K|\rho_{i,j}|^2\mathrm{Re}(\rho_{i,j})}{n^2(K+1)^4}\\ &+\sum_{i=1}^{n}\sum_{j=1,j\neq i}^{n}\frac{|\rho_{i,j}|^2(8K^2+8K+4) + 8K\mathrm{Re}(\rho_{i,j})}{n^2(K+1)^4}.\end{aligned} \tag{21}$$

Hence, we can write

$$\begin{aligned}G_a &= 1 + e_a,\\ G_v &= \frac{2K+1}{(1+K)^2} - \Delta + e_v,\end{aligned} \tag{22}$$

where the mean values of e_a and e_v are both zero and their variances are $\mathrm{Var}(G_a)$ and $\mathrm{Var}(G_v)$ respectively. Substituting (22) into (10), the estimated K-factor is

$$\hat{K} = \frac{\sqrt{(1+e_a)^2 - \frac{2K+1}{(K+1)^2} + \Delta - e_v}}{1 + e_a - \sqrt{(1+e_a)^2 - \frac{2K+1}{(K+1)^2} + \Delta - e_v}}. \tag{23}$$

Based on the derivations shown in Appendix B, we can obtain the bias of this K-factor estimator as shown in (61), which is related to the correlation coefficients, the number of samples and the K-factor itself. Inverting (23) allows us to obtain the true K-factor from the estimated K-factor as follows

$$K = \frac{\sqrt{1 + e_v - \Delta - \frac{(1+e_a)^2(2\hat{K}+1)}{(\hat{K}+1)^2}}}{1 - \sqrt{1 + e_v - \Delta - \frac{(1+e_a)^2(2\hat{K}+1)}{(\hat{K}+1)^2}}}. \tag{24}$$

However, it must be noted that Δ is a complex function of the true K-factor and the correlation coefficients so that only when Δ is negligible will this equation be useful.

B. Qualitative Analysis of the Bias

We have shown that the bias of the proposed K-factor estimator is related to the number of samples, n, the K-factor, K, and the correlation coefficient, $\rho_{i,j}$, contained in Δ and Δ'. To qualitatively analyze the relationship between these parameters, we can simplify (61) as

$$\mathrm{Bias} \approx \frac{d_1}{n} + \frac{d_2 K}{n} + d_3\Delta' K^3 + d_4\Delta K^2 + d_5\Delta^2 K^3, \tag{25}$$

where $d_i, i = 1, 2, ..., 5$ are positive constants. Some components that are smaller than the five components in (25) are neglected. The condition of this simplification is $K \geq 1$. This simplification is to allow intuitive interpretations, while simulations are done by using (61). When the spectral samples are uncorrelated and $\rho_{i,j}$ is zero, Δ, Δ' are correspondingly equal to zero. Hence, the bias is a function of K and n. Furthermore, the bias increases linearly with the K-factor while it decreases as the number of samples increases. The linear growth of the bias with the K-factor can be identified by inspection of the terms in (25). For example, there is a product of the positive constant, d_2, and the K-factor, K, in (25). Note that the terms involving K^2 and K^3 in (25) are multiplied by factors which reduce the order of the terms to linear in K or lower. Hence, the relationship is approximately linear. This can also be empirically explained as the bias is amplified when the estimated value increases. A similar trend is shown in [24], in which more samples are needed to get a certain standard deviation when the K-factor value increases. Specifically, when n is large and fixed, the bias is relatively small. On the other hand, if different spectral samples exhibit strong serial correlation, then, Δ and Δ' induce a larger bias. Generally, in the radio propagation channel, the correlation

This article has been accepted for publication in a future issue of this journal, but has not been fully edited. Content may change prior to final publication. Citation information: DOI 10.1109/TVT.2018.2878352, IEEE Transactions on Vehicular Technology

coefficients decrease as the spacing increases between two different samples. We finally note that the bias analysis is generally valid for K-factor estimates based on the moment method, no matter whether the underlying samples are spectral or temporal samples, or a combination thereof.

IV. Numerical Results

In this section, we conduct a series of simulations using equations (6)-(10) to verify the above results and verify the relationship between bias and other related parameters. According to (19), the variances of G_a and G_v are dependent on the number of samples, the true K-factor and the correlation coefficients. Hence, we use two possible scenarios to investigate the variance of G_a and G_v, correlated and uncorrelated. Uncorrelated samples are independent $CN(0,1)$ (complex normal) variables. Furthermore, Eq. (26) is used to create the correlation coefficient matrix, $\rho_{i,j}$ is the (i,j) entry of the matrix. Then, correlated samples are generated by multiplying the uncorrelated samples with the principal square root of the correlation coefficient matrix. In the simulations, the number of samples, n, is varied from 100 to 1000 with a stepsize of 50 and the K-factor, K, is varied from 1 to 100 with a stepsize of 2 on a linear scale. The correlation coefficients are created as follows [28]

$$\rho_{i,j} = \frac{1 + 2\pi j_c \tau_d \Delta f (i-j)}{1 + (2\pi\tau_d \Delta f (i-j))^2},\ i,j = 1,2...,n, \qquad (26)$$

where Δf is the frequency spacing, τ_d is the root mean square delay spread. Note that (26) gives the serial correlation across frequency for the particular scenario of an exponential power delay profile as discussed in [28] and [29]. Hence it is a physically motivated special case for use in simulations. Results are shown in Figs. 1-3. The dashed line represents the simulation results and the solid line represents the theoretical values according to (19). We can see that theoretical derivations fit well with the simulation results. The variance of G_v decreases more quickly than the variance of G_a as the K-factor increases while they decrease with similar speed as the number of samples increases.

Based on the agreement between simulations and analytical results, we can use the variance of G_a and variance of G_v to calculate the theoretical bias of the K-factor estimator according to (61). Firstly, we consider the situation where the samples are not correlated and thus Δ, $\Delta^{'}$ are equal to zero. Hence, the bias is only related to the number of samples, n, and the K-factor, K. Figure 4 shows the simulation results. In this simulation, n is set to 500. As the K-factor increases from 1 up to 100, the bias increases from around 0 to around 0.4 in an approximately linear fashion. Figure 5 shows the simulation results for $K = 10$. The bias decreases from around 0.25 to around 0.03 as n increases from 100 to 1000. Overall, when the successive samples are not correlated, as predicted by the analysis, the bias increases linearly as the K-factor ($K \geq 1$ on the linear scale) increases and it is an inverse function of the number of samples.

Secondly, when the successive samples are correlated, the bias also increases with the size of the correlation coefficient. Figure 6 shows the simulation results. In these simulations, n is set to 500 and K is set to 10 (linear scale). The correlation coefficient between successive samples are all set according to (26) by varying τ_d to give a desired value. $\rho_{1,2}$ represents the correlation coefficient between adjacent samples. We can see that the theoretical bias fits well with the simulated bias. Further, when the successive samples are very strongly correlated, e.g., $|\rho_{1,2}|$ is more than 0.98, the bias increases greatly as shown in Figure 6. Also, the bias is generally small when $|\rho_{1,2}|$ is less than 0.95. As shown in Figure 3, there is a small gap between theoretical and simulated bias values due to the simplifications in the derivations. In short, our derivations fit well with simulation results, and when the successive samples are strongly correlated, the correlation greatly increases the bias.

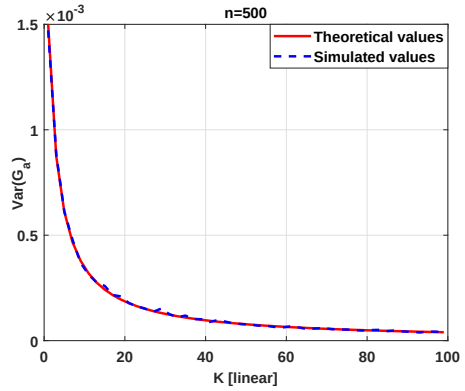

(a) Var(G_a) vs. K

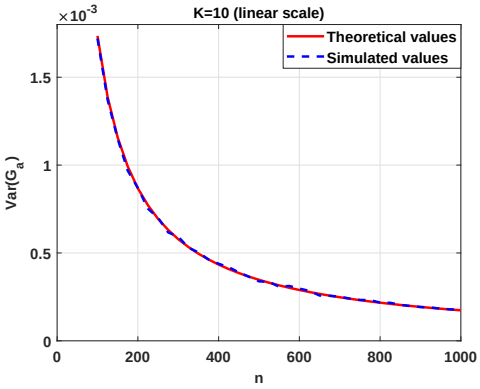

(b) Var(G_a) vs. n

Fig. 1. The variance of G_a under the condition of uncorrelated samples.

We have observed that the bias decreases with n and increases with correlation. Now, we consider the case of a fixed bandwidth, where n is increased leading to increased correlation. Here, there are competing trends and it is unclear how the bias will behave. In simulations, the frequency spacing, Δf, is set to $\frac{50}{n}$ MHz and τ_d is set to 50 ns, empirically. Hence, as n increases, the correlation between adjacent samples also increases. Simulation results are shown in Figure 7. We can see that when the number of samples increases for a fixed bandwidth, overall the bias remains almost constant.

The results shown suggest that our theoretical approximations of the bias of the proposed K-factor estimator perform

This article has been accepted for publication in a future issue of this journal, but has not been fully edited. Content may change prior to final publication. Citation information: DOI 10.1109/TVT.2018.2878352, IEEE Transactions on Vehicular Technology

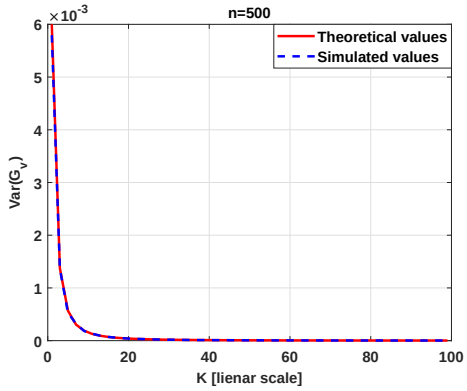

(a) Var(G_v) vs. K

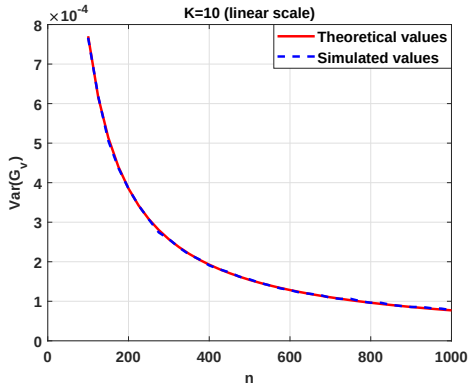

(b) Var(G_v) vs. n

Fig. 2. The variance of G_v under the condition of uncorrelated samples.

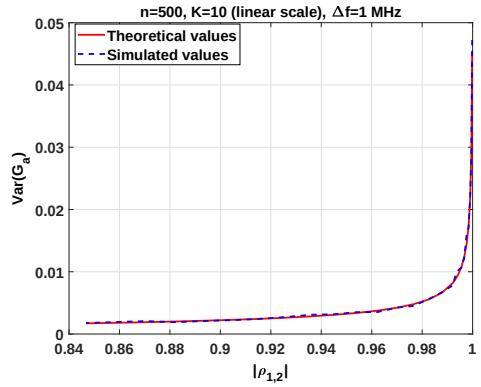

(a) Var(G_a) vs. $|\rho_{1,2}|$

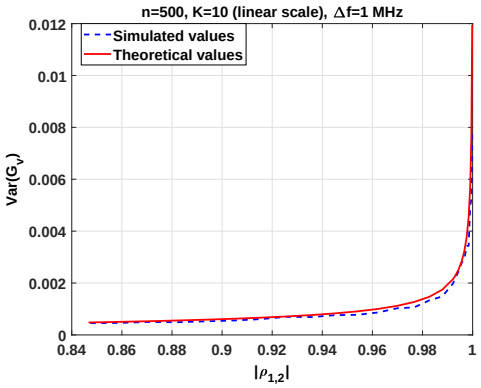

(b) Var(G_v) vs. $|\rho_{1,2}|$

Fig. 3. The relationship between the correlation and variances, Var(G_a) and Var(G_v), under the condition of correlated samples. $\rho_{1,2}$ represents the correlation coefficient between adjacent samples.

well when researching the relationship between the bias and related parameters, i.e., the number of envelope samples across the measurement bandwidth, the K-factor and the correlation coefficients. In the following sections, we use the proposed K-factor estimator to extract the K-factor from the measured data.

V. Measurement Setup and Scenario

A. Measurement Facilities

In this measurement campaign, a wideband correlation sounder was used to capture the channel information. The sounder consists of separate components, e.g., up-converter, down-converter, streaming disk and baseband block. The measurement bandwidth is 400 MHz. At the transmitter (TX) side, a pseudo-random (PN) noise sequence is generated as the probing signal with a chip rate of 200 MHz, and the pulse repetition interval is 5115 ns. Then, this baseband probing signal is frequency-shifted to 28 GHz by a complex up-converter. Before inputting the signal into the antenna, a power amplifier with a 1 dB compression point of 33 dBm, and a gain of 56 dB is used to make sure the maximum average output power before the TX antenna can be up to 30 dBm. At the receiver (RX) side, a low noise amplifier with a 1 dB compression point of 5 dBm and a gain of 20 dB is used to amplify the received signal. Subsequently, the complex down-converter converts the received signal to baseband. A streaming disk with a writing speed of 16 GB/s is used to

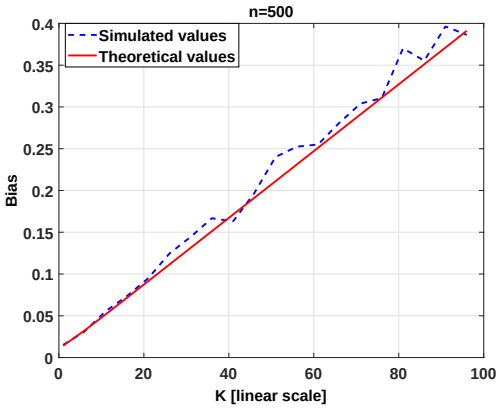

Fig. 4. The relationship between the bias and the true K-factor.

store the IQ data in real time. The CIRs in (3) can be obtained by correlating the IQ data with a stored measurement system back to back recording. Two rubidium clocks disciplined by global positioning system (GPS) signals are used at the TX and RX side separately. In terms of antennas, a 2 dBi biconical antenna (omnidirectional, and directional with 40° half-power beamwidth (HPBW), in azimuth and elevation, respectively) is used at the TX side and mounted on a trolley. At the RX side, an 8 dBi sectored antenna (90° and 40° HPBW in azimuth and elevation, respectively) is used. Detailed measurement settings

This article has been accepted for publication in a future issue of this journal, but has not been fully edited. Content may change prior to final publication. Citation information: DOI 10.1109/TVT.2018.2878352, IEEE Transactions on Vehicular Technology

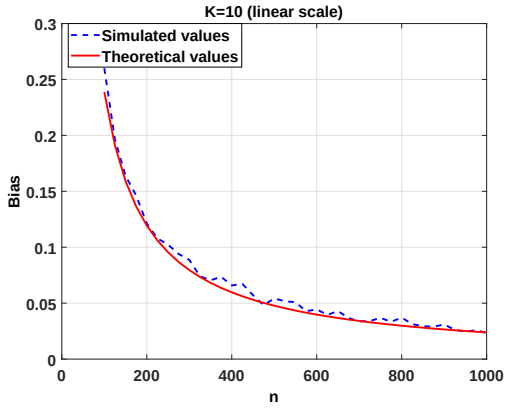

Fig. 5. The relationship between the bias and the number of samples.

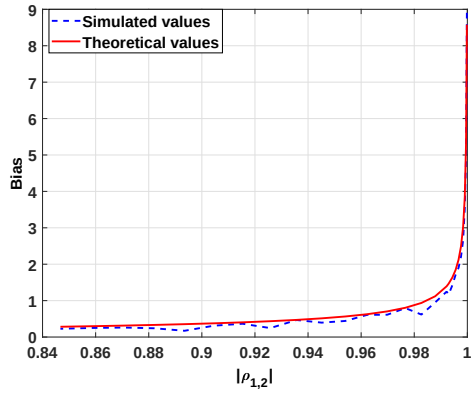

Fig. 6. The relationship between the bias and the correlation coefficient.

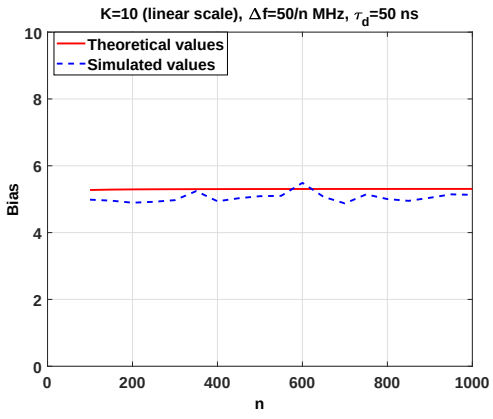

Fig. 7. The relationship between the bias and the number of samples under the same bandwidth.

(a) The real measurement environment

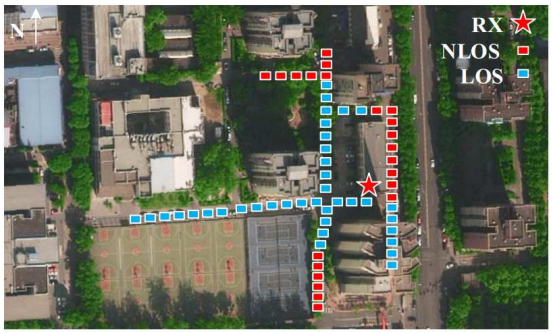

(b) The distribution of measurement routes

Fig. 8. The schematic diagram of the measured positions.

are summarized in Table I.

TABLE I
MEASUREMENT SETTING

Property	Values
Central frequency	28 GHz
Bandwidth	400 MHz
PN sequence	1023
Delay resolution	5 ns
Max output power	30 dBm
TX/RX antenna type	Biconical/Sectored
TX/RX antenna gain	2 dBi/8 dBi
TX/RX antenna polarization	Vertical
TX/RX antenna azimuth HPBW	Omnidirectional/90°
TX/RX antenna elevation HPBW	40°/40°
TX/RX antenna height	1.66 m/13.38 m

B. Measurement Scenario

The measurements were conducted in an urban micro-cell scenario at the Beijing University of Posts and Telecommunications campus [30] [31]. The TX was put on the ground while the RX was fixed on the roof of a building with a height of 11.75 m. The heights of TX and RX antennas were 1.66 m and 13.38 m respectively. There were many high buildings around the RX. A photograph of the measurement environment is shown in Figure 8(a). We conducted two types of measurements: fixed-location measurements and time-series

This article has been accepted for publication in a future issue of this journal, but has not been fully edited. Content may change prior to final publication. Citation information: DOI 10.1109/TVT.2018.2878352, IEEE Transactions on Vehicular Technology

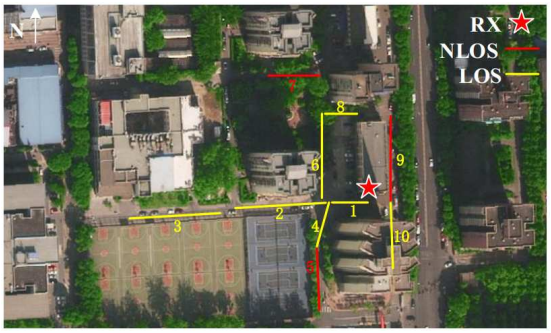

Fig. 9. The schematic diagram of the measured routes.

measurements. During the fixed-location measurements, the TX was mounted on the trolley and fixed on the ground. The spacing of the successive measured positions was 2 m. The GPS antenna was used to record the position information of the TX. There were in total 138 LOS measured positions and 101 NLOS measured positions. The measured distance range of the LOS positions was 18.9 m up to 148.94 m while it was 12.69 m up to 78.59 m for the NLOS positions. Figure 8(b) shows the schematic diagram of the measured positions. During the time-series measurements, the trolley on which the TX was mounted was pushed along the planned routes with a speed of around 1 m/s. There were 10 routes in total including 7 LOS routes and 3 NLOS routes. The schematic diagram of the measured routes is shown in Figure 9.

VI. Estimating the K-factor in time and frequency domain based on the time-series measurements

In addition to the theoretical derivations in Section III and the simulation in Section IV used to support the proposed method, we also verify our method based on an analysis of measured time series data. Two methods, the typical method and the proposed method discussed in Section III, are used to estimate the K-factor.

The statistics of the K-factor extracted by these two methods from the time-series measurements are shown in Figure 10. The narrowband method, i.e, the typical method, estimates the K-factor with a mean value of 9.35 dB in a LOS scenario (2.1 dB in a NLOS scenario) while the wideband method, i.e., the proposed method, estimates the K-factor with a mean value of 9.2 dB in a LOS scenario (2.62 dB in a NLOS scenario). Hence, the two different estimation methods can provide similar statistical results with measured data, supporting the analytical arguments. Next, we further compare the results in each route and find that though the estimation results obtained by these two methods have a similar trend and mean value, there exists a discrepancy in the estimated K-factor in some regions. For example, as shown in Figure 11, these two methods can give almost the same K-factor value in some stationarity regions while the discrepancy in some stationarity regions is large. We empirically suggest that the discrepancy may arise from the following reasons:

- The number of samples in the time domain is not the same as that in frequency. In frequency, because of the limited bandwidth, the number of samples is relatively small compared to the time domain.
- The correlation coefficients of samples in frequency are not the same as in time.
- Artificial effects. During measurements, the trolley is manually pushed along the route and we assume the moving speed is constant. However this assumption may not be realistic especially over uneven ground, which may bring about changes in correlation.

VII. The Statistical Analysis of the K-factor based on the fixed-location measurements

The analysis in Section II assumes that the channel TFEs obtained from the measured data can be modeled by a Ricean distribution as in (5). Hence, before using the proposed K-factor estimator, we need to investigate if this assumption holds for our data. For this purpose, we use the Kolmogorov Smirnoff (KS) test statistic to measure the goodness of fit [32]. Note that serial correlation among the TFEs is likely and the parameters of the Ricean have to be estimated. Under these conditions, it is known that the KS test is conservative [33], [34]. The KS test statistic is defined as

$$D_{\max} = \max(|F(|H_i|) - G(|H_i|)|), \tag{27}$$

where $G(|H_i|)$ is the empirical CDF of $|H_i|$ and $F(|H_i|)$ is the CDF of the Ricean fit. Another test output is the P-value, which is the probability of observing a test statistic as extreme as, or more extreme than, the observed value under the null hypothesis. The KS test decides whether to reject the null hypothesis by comparing the P with the significance level, α. Commonly, α is set to 0.05. In our KS test, the samples in each LOS and NLOS position are used to perform the KS test. Figure 12 shows the KS test results. We can see that 50% of the values of $D_{\max}$ are smaller than 0.12 and most are smaller than 0.17. Besides, as shown in Figure 12(b), only 1 percent of the P-values are smaller than the significance level, α, and reject the null hypothesis of a Ricean distribution. In general, these KS test results are consistent with a Ricean model, particularly since the test is conservative in these conditions. Therefore we use the proposed estimator to calculate the K-factor.

As shown in Figure 6 for the example correlation in (26), which is a function of root mean square delay spread and frequency spacing, the bias of the proposed K-factor estimator is relatively small when the correlation coefficient between adjacent samples satisfies $|\rho_{1,2}| \leq 0.95$. However, when $|\rho_{1,2}| \geq 0.98$, the bias increases greatly, as shown in Figure 6. Hence, to reduce the effects of bias on estimation accuracy in the measurement, we choose TFEs separated by the value of frequency spacing for which the modulus of the sample autocorrelation function drops below 0.95. Correspondingly, we set 1 MHz as the spacing of selected successive spectral positions. Figure 13 shows the statistics of the K-factor (in dB) extracted by our proposed method in the urban micro-cell scenario. We can see that the K-factor (in dB) of both LOS and NLOS scenarios can be fitted well with a normal (Gaussian) distribution. As shown in Figure 13(a), the mean value of the normal fitting is 9.72 dB, which is close to the 9 dB obtained

This article has been accepted for publication in a future issue of this journal, but has not been fully edited. Content may change prior to final publication. Citation information: DOI 10.1109/TVT.2018.2878352, IEEE Transactions on Vehicular Technology

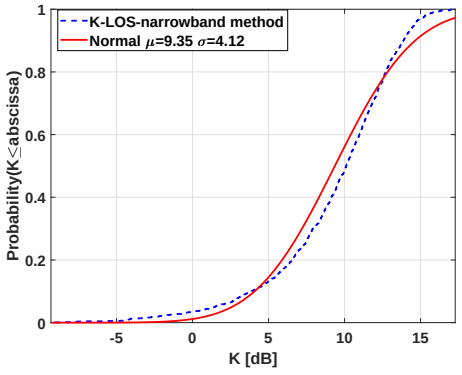

(a)

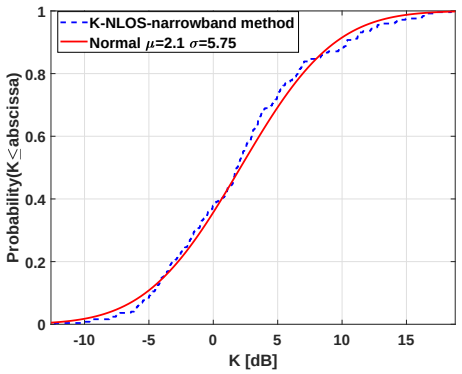

(b)

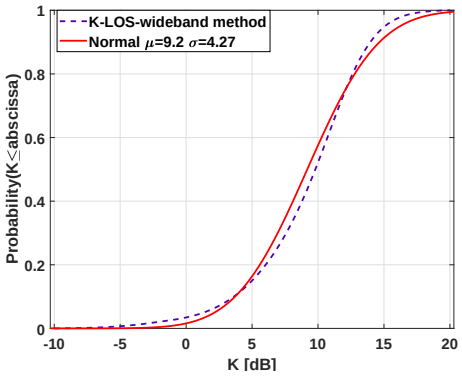

(c)

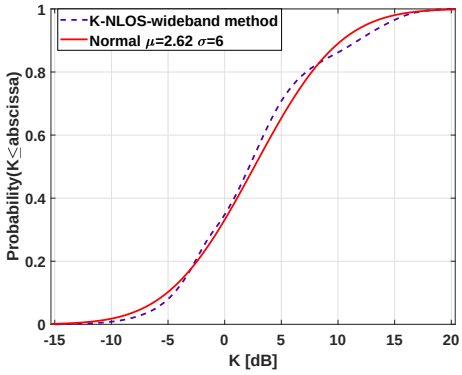

(d)

Fig. 10. The statistical results of the K-factor extracted by: a) narrowband method in the LOS scenarios; b) narrowband method in the NLOS scenarios; c) wideband method in the LOS scenarios; d) wideband method in the NLOS scenarios.

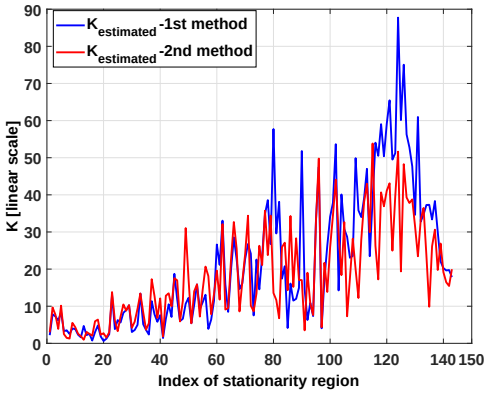

Fig. 11. The estimated K-factor in the 1st route using two different methods.

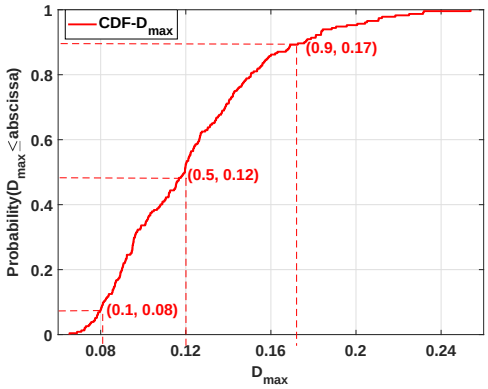

(a) The KS test statistic $D_{\max}$

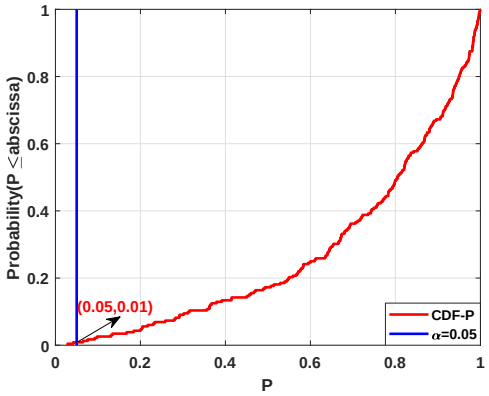

(b) The KS test statistic P-value

Fig. 12. The KS test results.

in [35]. The small difference is conjectured to be mainly due to the difference in the measured environment. For the K-factor results in the NLOS scenario, shown in Figure 13(b), the mean value of the normal fitting is 2.23. This suggests that in NLOS situations, Ricean variations can still result if the received signal contains a deterministic specular reflection. Furthermore, on fixed radio links Ricean variations can result if there is neither LOS, nor a specular component, depending on the length of time the received signal is observed, which is a non-stationary process. This is because regardless of

This article has been accepted for publication in a future issue of this journal, but has not been fully edited. Content may change prior to final publication. Citation information: DOI 10.1109/TVT.2018.2878352, IEEE Transactions on Vehicular Technology

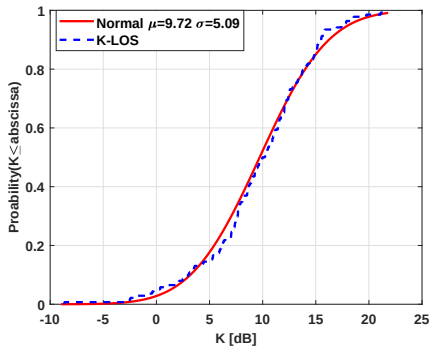

(a) The LOS K-factor results

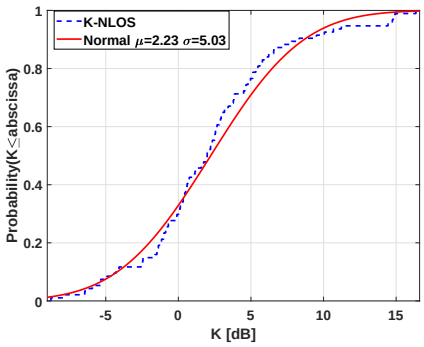

(b) The NLOS K-factor results

Fig. 13. The statistics of the K-factor. Each position has a K-factor estimate, and there are 138 K-factor estimates in LOS scenario and 101 K-factor estimates in NLOS scenario.

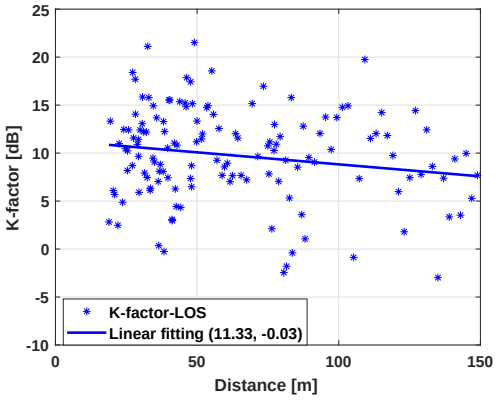

(a) The LOS scenario

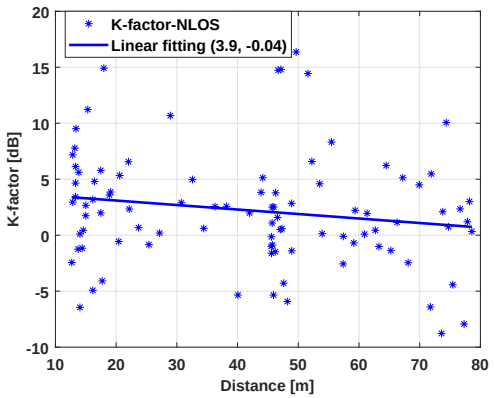

(b) The NLOS scenario

Fig. 14. The relationship between the K-factor and distance.

conditions between the TX and RX, after each perturbation of the received signal, the vector sum of the received signals returns to exactly the same amplitude and phase each time the perturbation stops [36]. Similar effects have been observed in the below-6 GHz range [37].

To characterize distance dependence of the K-factor, we model the relationship between the K-factor in dB and distance in meters by a linear model

$$K = a + b \cdot d + Z, Z \sim N(0, \sigma^2), \tag{28}$$

where d is the Euclidean distance between TX and RX, a is a constant, b is the distance-dependent exponent and Z is a random Gaussian variable. Figure 14 shows the linear fitting results where (a, b) refers to the estimates of the parameters in (28). The blue line is the linear fit. We can see that the slopes of the LOS and NLOS linear fits are -0.03 and -0.04 respectively. Furthermore, 95% confidence intervals for the slope estimates are $(-0.05, 0)$ and $(-0.09, 0.01)$, respectively. For the LOS scenario, the upper confidence bound for the slope is zero so that we can conclude that as the distance increases, the K-factor in the LOS scenario decreases. This can be explained physically by the fact that as the distance increases, the LOS component power decreases according to the free-space pathloss law. However, the reflected or scattered components increase relatively speaking, as the complexity of the environment between RX and TX increases, and the K-factor decreases correspondingly. For the NLOS scenario, the confidence interval for the slope includes zero and there is less evidence that the K-factor decreases as the distance increases. However, zero is close to the upper bound and a 90% interval does not include zero. More measurement results are needed to investigate this trend. Table II summarizes the statistics of the K-factor in this urban micro-cell scenario at 28 GHz.

TABLE II
THE STATISTICS OF THE K-FACTOR IN AN URBAN MICRO-CELL SCENARIO AT 28 GHZ.

Scenarios		Urban micro-cell	
		LOS	NLOS
K [dB]	μ	9.72	2.23
	σ	5.09	5.03
K [dB] - d [m]	a	11.33	3.9
	b	-0.03	-0.04
	σ	5.01	4.95

VIII. CONCLUSION

In this paper, we apply the moment-method estimator to the frequency domain to calculate the K-factor for narrowband temporal selectivity from the wideband measured data. The K-factor is extracted from the ensemble of narrowband channel transfer function estimates. The theoretical bias of a

This article has been accepted for publication in a future issue of this journal, but has not been fully edited. Content may change prior to final publication. Citation information: DOI 10.1109/TVT.2018.2878352, IEEE Transactions on Vehicular Technology

moment-method estimator is derived. We find that the bias is approximately linear with the K-factor ($K \geq 1$ on the linear scale) and is an inverse function of the number of the samples. It can be found that the bias is relatively small when the absolute value of the correlation coefficient between adjacent samples is less than 0.95. Otherwise, the bias increases greatly as the correlation increases. For a fixed bandwidth, as the number of samples increases and the correlation between adjacent samples increases correspondingly, the bias is almost constant. The statistics of a millimeter wave channel K-factor in an urban micro-cell scenario are extracted by using the proposed estimator on measured data. The K-factor in both LOS and NLOS scenarios can be modeled well by a lognormal distribution. Furthermore, the relationship between the K-factor and distance is modeled as a linear dependence and for the LOS scenario, the K-factor decreases slowly as the distance increases.

APPENDIX A
THE MOMENTS OF G_a AND G_v

In this part, we compute the moments of G_a and G_v. It is easy to calculate

$$\mathrm{E}(G_a) = \frac{1}{n}\sum_{i=1}^{n}\mathrm{E}(|H_i|^2) = 1. \tag{29}$$

For the mean of G_v, we can write

$$\begin{aligned}\mathrm{E}(G_v) =& \frac{1}{n}\left(\sum_{i=1}^{n}\mathrm{E}(|H_i|^4)\right) - \frac{1}{n}\left(\sum_{i=1}^{n}\sum_{j=1}^{n}\mathrm{E}(|H_i|^2|H_j|^2)\right)\\ =& \frac{1}{n}\left(\sum_{i=1}^{n}\mathrm{E}(|H_i|^4)\right)\\ &- \frac{1}{n}\left(\sum_{i=1}^{n}\mathrm{E}(|H_i|^4) + \sum_{i=1}^{n}\sum_{j=1,j\neq i}^{n}\mathrm{E}(|H_i|^2|H_j|^2)\right)\\ =& \frac{2K+1}{(K+1)^2}\\ &- \frac{1}{n(n-1)}\sum_{i=1}^{n}\sum_{j=1,j\neq i}^{n}\frac{2K\mathrm{Re}(\rho_{i,j}) + |\rho_{i,j}|^2}{(K+1)^2},\end{aligned} \tag{30}$$

where $\rho_{i,j}$ is the correlation coefficient between the $j-th$ and $i-th$ samples and Re() returns the real part. For simplicity, we use Δ to represent $\frac{1}{n(n-1)}\sum_{i=1}^{n}\sum_{j=1,j\neq i}^{n}\frac{2K\mathrm{Re}(\rho_{i,j})+|\rho_{i,j}|^2}{(K+1)^2}$. Then, the variance of G_a can be calculated as

$$\begin{aligned}\mathrm{Var}(G_a) =& \mathrm{E}(G_a^2) - \mathrm{E}(G_a)^2\\ =& 1 + \frac{2K+1}{(K+1)^2} + \left(1-\frac{1}{n}\right)\Delta - 1\\ =& \frac{2K+1}{(K+1)^2} + \left(1-\frac{1}{n}\right)\Delta.\end{aligned} \tag{31}$$

In terms of the variance of G_v, we can write

$$\mathrm{Var}(G_v) = \mathrm{E}(G_v^2) - \mathrm{E}(G_v)^2, \tag{32}$$

where $\mathrm{E}(G_v)$ has been calculated in (30) and $\mathrm{E}(G_v^2)$ can be calculated by

$$\begin{aligned}\mathrm{E}(G_v^2) =& \frac{1}{n^2}\left(\sum_{i=1}^{n}\sum_{j=1}^{n}\mathrm{E}(|H_i|^4|H_j|^4)\right) +\\ &\frac{1}{n^2(n-1)^2}\left(\sum_{i=1}^{n}\sum_{j=1,j\neq i}^{n}\sum_{r=1}^{n}\sum_{s=1,s\neq r}^{n}\mathrm{E}(|H_i|^2|H_j|^2|H_r|^2|H_s|^2)\right)\\ &+\frac{2}{n^2(n-1)}\left(\sum_{i=1}^{n}\sum_{r=1}^{n}\sum_{s=1,s\neq r}^{n}\mathrm{E}(|H_i|^4|H_r|^2|H_s|^2)\right),\end{aligned} \tag{33}$$

where H_i, H_j, H_r and H_s are correlated with each other. In principle, this equation is possible to calculate, but it is very messy in practise. To simplify the derivations, we replace the sample variance, G_v, by the sample variance, $\widetilde{G}_v$, which assumes that the true mean, $\mathrm{E}[|H_i|^2] = 1$, is used instead of the sample mean, $\frac{1}{n}\sum_{i=1}^{n}|H_i|^2$,

$$\widetilde{G}_v = \frac{1}{n}\sum_{i=1}^{n}(|H_i|^4 - 2|H_i|^2 + 1). \tag{34}$$

Using $\widetilde{G}_v$ provides a best case scenario as using (9) can only provide more error. Furthermore, using (34) avoids the need to calculate $8-th$ order joint moments. Then, we can get

$$\begin{aligned}\mathrm{E}(\widetilde{G}_v^2) =& \frac{1}{n^2}\left(\sum_{i}^{n}\mathrm{E}(|H_i|^8) + \sum_{i}^{n}\sum_{j,j\neq i}^{n}\mathrm{E}(|H_i|^4|H_j|^4)\right)\\ &+\frac{1}{n^2}\left(-4\sum_{i=1}^{n}\mathrm{E}(|H_i|^6) - 4\sum_{i}^{n}\sum_{j,j\neq i}^{n}\mathrm{E}(|H_i|^4|H_j|^2)\right)\\ &+\frac{1}{n^2}\left((4+2n)\sum_{i=1}^{n}\mathrm{E}(|H_i|^4) - 4n\sum_{i=1}^{n}\mathrm{E}(|H_i|^2) + n^2\right)\\ &+\frac{1}{n^2}\left(4\sum_{i}^{n}\sum_{j,j\neq i}^{n}\mathrm{E}(|H_i|^2|H_j|^2)\right).\end{aligned} \tag{35}$$

In the above equation, the mean values of some of the more complex parts are listed as follows

$$\mathrm{E}(|H_i|^8) = \frac{K^4+16K^3+72K^2+96K+24}{(K+1)^4}, \tag{36}$$

$$\begin{aligned}\mathrm{E}(|H_i|^4|H_j|^4) =& \frac{K^4+8K^3+20K^2+16K+4}{(K+1)^4}\\ &+\frac{\mathrm{Re}(\rho_{i,j})(8K^3+32K^2+32K)}{(K+1)^4}\\ &+\frac{|\rho_{i,j}|^2(16K^2+32K+16)+2K^2(\rho_{i,j}^2+\rho_{i,j}^{*\,2})}{(K+1)^4}\\ &+\frac{|\rho_{i,j}|^2\mathrm{Re}(\rho_{i,j})16K+|\rho_{i,j}|^4 4}{(K+1)^4},\end{aligned} \tag{37}$$

This article has been accepted for publication in a future issue of this journal, but has not been fully edited. Content may change prior to final publication. Citation information: DOI 10.1109/TVT.2018.2878352, IEEE Transactions on Vehicular Technology

$$\mathrm{E}(|H_i|^4|H_j|^2) = \frac{K^3+5K^2+6K+2}{(K+1)^3} + \frac{\mathrm{Re}(\rho_{i,j})(4K^2+8K)+|\rho_{i,j}|^2(4K+4)}{(K+1)^3}. \tag{38}$$

Based on the above derivations, the variance of G_v can be obtained as

$$\begin{aligned}\mathrm{Var}(\widetilde{G}_v) &= \frac{8K^2+32K+8}{n(K+1)^4} \\ &+ \sum_{i=1}^{n}\sum_{j=1,j\neq i}^{n} \frac{4|\rho_{i,j}|^4+16K|\rho_{i,j}^2|\mathrm{Re}(\rho_{i,j})}{n^2(K+1)^4} \\ &+ \sum_{i=1}^{n}\sum_{j=1,j\neq i}^{n} \frac{|\rho_{i,j}|^2(4K^2+8K+4)+8K\mathrm{Re}(\rho_{i,j})}{n^2(K+1)^4} \\ &+ \sum_{i=1}^{n}\sum_{j=1,j\neq i}^{n} \frac{2K^2(\rho_{i,j}^2+{\rho_{i,j}^*}^2)}{n^2(K+1)^4} \\ &= \frac{8K^2+32K+8}{n(K+1)^4} + \Delta^{'},\end{aligned} \tag{39}$$

where $\Delta^{'}$ is used to represent the part containing correlation coefficients.

In the derivations of bias, the mean value of G_aG_v is needed. According to (34), we replace G_aG_v by $G_v\widetilde{G}_v$ so that

$$G_a\widetilde{G}_v = \frac{1}{n^2}\left(\sum_{i=1}^{n}|H_i|^6 + \sum_{i=1}^{n}\sum_{j=1,j\neq i}^{n}|H_i|^4|H_j|^2\right) + \frac{1}{n^2}\left(n\sum_{i=1}^{n}|H_i|^2 - 2\sum_{i=1}^{n}|H_i|^4 - 2\sum_{i=1}^{n}\sum_{j=1,j\neq i}^{n}|H_i|^2|H_j|^2\right). \tag{40}$$

Hence, the mean value of G_aG_v can be obtained by

$$\mathrm{E}(G_a\widetilde{G}_v) = \frac{6K+2}{(K+1)^3n} + \frac{2K+1}{(K+1)^2} + \sum_{i=1}^{n}\sum_{j=1,j\neq i}^{n}\frac{|\rho_{i,j}|^2(2K+2)+\mathrm{Re}(\rho_{i,j})4K}{n^2(K+1)^3}. \tag{41}$$

Appendix B
The Derivation of the Bias of the K-factor Estimator

According to (22), the estimated K-factor can be written as

$$\hat{K} = \frac{\sqrt{(\frac{K}{K+1})^2+2e_a+e_a^2+\Delta-e_v}}{1+e_a-\sqrt{(\frac{K}{K+1})^2+2e_a+e_a^2+\Delta-e_v}}. \tag{42}$$

Multiplying the numerator and denominator by $1+e_a+\sqrt{(\frac{K}{K+1})^2+2e_a+e_a^2+\Delta-e_v}$ and using X to represent $2e_a+e_a^2+\Delta-e_v$ yields

$$\hat{K} = \frac{(1+e_a)(K+1)\sqrt{K^2+X(K+1)^2}+K^2+X(K+1)^2}{(2K+1)(1+\frac{(e_v-\Delta)(K+1)^2}{2K+1})}. \tag{43}$$

Considering that the value of e_a is small compared with 1, the part $(1+e_a)$ approximately equals 1. Then, using the Taylor formula to simplify (43),

$$\begin{aligned}(K+1)\sqrt{K^2+X(K+1)^2} &= K(K+1)\sqrt{1+X(\frac{K+1}{K})^2} \\ &= K(K+1)(1+\frac{X}{2}(\frac{K+1}{K})^2 - \frac{X^2}{8}(\frac{K+1}{K})^4)+...),\end{aligned} \tag{44}$$

where $|X(\frac{K+1}{K})^2|$ is smaller than 1. For the denominator, we can get

$$\left(1+\frac{(e_v-\Delta)(K+1)^2}{2K+1}\right)^{-1} = 1-\frac{(e_v-\Delta)(K+1)^2}{2K+1} + \frac{(e_v-\Delta)^2(K+1)^4}{(2K+1)^2}+.... \tag{45}$$

Substituting (45) and (44) into (43) yields

$$\hat{K} \approx \frac{(2K^2+K+A+C)(1+B)}{2K+1}, \tag{46}$$

where $A = X\frac{(K+1)^2(3K+1)}{2K} - X^2\frac{(K+1)^5}{8K^3}$, $B = -(e_v-\Delta)\frac{(K+1)^2}{2K+1} + (e_v-\Delta)^2\frac{(K+1)^4}{(2K+1)^2}$ and $C = e_a(1+X\frac{(K+1)^2}{2K^2} - X^2\frac{(K+1)^4}{8K^4})K(K+1)$. Then, we can get the bias as follows:

$$\begin{aligned}\mathrm{Bias} &= \mathrm{E}(\hat{K}-K) \\ &\approx \mathrm{E}(KB) + \frac{\mathrm{E}(A)+\mathrm{E}(AB)+\mathrm{E}(C)+\mathrm{E}(BC)}{2K+1}.\end{aligned} \tag{47}$$

Now, we can see that the bias is related to the K-factor, the number of samples and the correlation coefficients between successive samples. Then, we compute the mean values of A, B, C AB and BC as follows

$$\mathrm{E}(A) = \frac{\mathrm{E}(X)(3K+1)(K+1)^2}{2K} - \frac{\mathrm{E}(X^2)(K+1)^5}{8K^3}, \tag{48}$$

$$\mathrm{E}(B) = \frac{\mathrm{E}(\Delta-e_v)(K+1)^2}{2K+1} + \frac{\mathrm{E}((\Delta-e_v)^2)(K+1)^4}{(2K+1)^2}, \tag{49}$$

$$\begin{aligned}\mathrm{E}(AB) &= \frac{\mathrm{E}(X(\Delta-e_v))(K+1)^4(3K+1)}{2K(2K+1)} \\ &+ \frac{\mathrm{E}(X(\Delta-e_v)^2)(K+1)^6(3K+1)}{2K(2K+1)^2} \\ &- \frac{\mathrm{E}(X^2(\Delta-e_v))(K+1)^7}{8K^3(2K+1)} \\ &- \frac{\mathrm{E}(X^2(\Delta-e_v)^2)(K+1)^9}{8K^3(2K+1)^2},\end{aligned} \tag{50}$$

$$\mathrm{E}(C) = \frac{(K+1)^3}{2K}\mathrm{E}(Xe_a) - \frac{(K+1)^5}{8K^3}\mathrm{E}(X^2e_a), \tag{51}$$

$$\begin{aligned}\mathrm{E}(BC) &= \frac{\mathrm{E}(-e_ve_a)K(K+1)^3}{2K+1} + \frac{\mathrm{E}((\Delta-e_v)^2e_a)K(K+1)^5}{(2K+1)^2} \\ &+ \frac{\mathrm{E}((\Delta-e_v)Xe_a)(K+1)^5}{2K(2K+1)} + \frac{\mathrm{E}((\Delta-e_v)^2Xe_a)(K+1)^7}{2K(2K+1)^2} \\ &- \frac{\mathrm{E}((\Delta-e_v)X^2e_a)(K+1)^7}{8K^3(2K+1)} - \frac{\mathrm{E}((\Delta-e_v)^2X^2e_a)(K+1)^9}{8K^3(2K+1)^2}.\end{aligned} \tag{52}$$

This article has been accepted for publication in a future issue of this journal, but has not been fully edited. Content may change prior to final publication. Citation information: DOI 10.1109/TVT.2018.2878352, IEEE Transactions on Vehicular Technology

In the following equations, for simplicity, let V_1 and V_2 represent the variances of G_a and G_v respectively, V_3 is the mean value of $e_a e_v$. We can show that Δ is equal to $O(\frac{1}{n})$, e_a and e_v are equal to $O(\frac{1}{\sqrt{n}})$ and e_a^2 and e_v^2 are equal to $O(\frac{1}{n})$ using the classical mathematical notation for the limiting behavior of a function. In the following derivations, we keep the terms consisting of V_1, V_2, V_3 or Δ and other smaller terms are neglected.

$$\begin{aligned} &\mathrm{E}(X) = V_1 + \Delta, \\ &\mathrm{E}(X^2) \approx 4V_1 + V_2 + 2\Delta V_1 - 4V_3 + \Delta^2. \end{aligned} \tag{53}$$

Before calculating $E(AB)$, we firstly compute the following components.

$$\begin{aligned} &\mathrm{E}(X(\Delta - e_v)) \approx V_2 + \Delta V_1 - 2V_3 + \Delta^2, \\ &\mathrm{E}(X(\Delta - e_v)^2) \approx 3\Delta V_2 - 4\Delta V_3 + \Delta^2 V_1 + \Delta^3, \\ &\mathrm{E}(X^2(\Delta - e_v)^2) \approx 4\Delta^2 V_1 + 6\Delta^2 V_2 - 8\Delta^2 V_3 + 2\Delta^3 V_1 + \Delta^4, \\ &\mathrm{E}(X^2(\Delta - e_v)) \approx 4\Delta V_1 + 3\Delta V_2 - 8\Delta V_3 + 2\Delta^2 V_1 + \Delta^3. \end{aligned} \tag{54}$$

In terms of $E(BC)$, we should calculate the following components

$$\begin{aligned} &\mathrm{E}(X(\Delta - e_v)e_a) \approx 2\Delta V_1 - 2\Delta V_3, \\ &\mathrm{E}(X(\Delta - e_v)^2 e_a) \approx -3\Delta^2 V_3, \\ &\mathrm{E}(X^2(\Delta - e_v)^2 e_a) \approx 4\Delta^2 V_1 - 3\Delta^2 V_3, \\ &\mathrm{E}(X^2(\Delta - e_v)e_a) \approx -4\Delta^3 V_3. \end{aligned} \tag{55}$$

Then, we keep all $O(\frac{1}{n})$ terms and remove smaller terms. The term Δ^2 is kept because, although it has lower order, the impact of the correlations may make it non-negligible for reasonable sized values or n. Combining with (53), (54), (55), we can get

$$\frac{\mathrm{E}(BC)}{2K+1} \approx -V_3 \frac{K(K+1)^3}{(2K+1)^2}, \tag{56}$$

$$\frac{\mathrm{E}(C)}{2K+1} \approx V_1 \frac{(K+1)^3}{K(2K+1)} - V_3 \frac{(K+1)^3}{2K(2K+1)}, \tag{57}$$

$$\begin{aligned} \frac{\mathrm{E}(A)}{2K+1} \approx\ & V_1 \frac{(K+1)^2(2K^3 - 2K^2 - 3K - 1)}{2K^3(2K+1)} \\ & - V_2 \frac{(K+1)^5}{8K^3(2K+1)} + V_3 \frac{(K+1)^5}{2K^3} \\ & + \Delta \frac{(3K+1)(K+1)^2}{2K(2K+1)}, \end{aligned} \tag{58}$$

$$\mathrm{E}(KB) = V_2 \frac{K(K+1)^4}{(2K+1)^2} + \Delta \frac{K(K+1)^2}{2K+1} + \Delta^2 \frac{K(K+1)^4}{(2K+1)^2}, \tag{59}$$

$$\frac{\mathrm{E}(AB)}{2K+1} \approx V_2 \frac{(K+1)^4(3K+1)}{2K(2K+1)^2} - V_3 \frac{(K+1)^4(3K+1)}{K(2K+1)^2}. \tag{60}$$

Substituting (56)-(60) into (47) yields

$$\begin{aligned} \text{Bias} \approx\ & V_1 \frac{(K+1)^2(4K^3 - 3K - 1)}{2K^3(2K+1)} \\ & + V_2 \frac{(K+1)^4(8K^4 + 12K^3 + 2K^2 - 3K - 1)}{8K^3(2K+1)^2} \\ & + V_3 \frac{(K+1)^3(-8K^4 - 8K^3 + 2K^2 + 4K + 1)}{2K^3(2K+1)^2} \\ & \Delta \frac{(K+1)^3}{2K} + \Delta^2 \frac{K(K+1)^4}{(2K+1)^2}, \end{aligned} \tag{61}$$

where V_1, V_2 and Δ are given in Appendix A. We now need to calculate V_3, which is the mean value of $e_a e_v$. According to (34) (41), we can get

$$\begin{aligned} \mathrm{E}(e_a e_v) =& \mathrm{E}(G_a G_v) - \mathrm{E}(G_a)\mathrm{E}(G_v) \\ \approx& \mathrm{E}(G_a \widetilde{G}_v) - \mathrm{E}(G_a)\mathrm{E}(\widetilde{G_v}) \\ =& \frac{6K+2}{(K+1)^3 n} \\ & + \sum_{i=1}^{n} \sum_{j=1, j\neq i}^{n} \frac{|\rho_{i,j}|^2(2K+2) + \mathrm{Re}(\rho_{i,j})4K}{n^2(K+1)^3}. \end{aligned} \tag{62}$$

Now, the bias is known.

ACKNOWLEDGMENT

The work of the Chinese authors is supported by the National Natural Science Foundation of China (Grant No. 61322110), the Key program of Beijing Municipal Natural Science Foundation (Grant NO. L172030), the National Science and Technology Major Project of the Ministry of Science and Technology (Grant No. 2018ZX03001031), the Exploratory Project of State Key Lab of Networking and Switching Technology (Grant No. NST20170205) and National Key Technology Research and Development Program of the Ministry of Science and Technology of China (Grant No. 2012BAF14B01). The work of A. F. Molisch was supported by the National Institute of Standards and Technology (NIST) and the National Science Foundation (NSF).

REFERENCES

[1] A. F. Molisch. "Wireless Communications," 2nd edition, IEEE Press - Wiley, 2011.

[2] C. Lemoine, E. Amador and P. Besnier, "On the K-Factor Estimation for Rician Channel Simulated in Reverberation Chamber," in IEEE Transactions on Antennas and Propagation, vol. 59, no. 3, pp. 1003-1012, March 2011.

[3] D. Dong, J. Zhang, Y. Zhang and X. Nie, "Large Scale Characteristics and Capacity Evaluation of Outdoor Relay Channels at 2.35 GHz," 2009 IEEE 70th Vehicular Technology Conference Fall, Anchorage, AK, 2009, pp. 1-5.

[4] S. Catreux, V. Erceg, D. Gesbert and R. W. Heath, "Adaptive Modulation and MIMO Coding for Broadband Wireless Data Networks," in IEEE Communications Magazine, vol. 40, no. 6, pp. 108-115, Jun 2002.

[5] X. Yu, S. H. Leung, W. Xu, X. Dang, Z. Luo and Y. Wang, "Precoding Design for Distributed Antenna Systems in Spatially Correlated Ricean Fading Channel," in IEEE Transactions on Vehicular Technology, vol.PP, no.99, pp.1-1

[6] H. Tataria, P. J. Smith, L. J. Greenstein, P. A. Dmochowski and M. Shafi, "Performance and Analysis of Downlink Multiuser MIMO Systems with Regularized Zero-Forcing Precoding in Ricean Fading Channels," 2016 IEEE International Conference on Communications (ICC), Kuala Lumpur, 2016, pp. 1-7.

[7] S. Sun, T. Rappaport, M. Shafi, P. Tang, J. Zhang and P. J. Smith, "Propagation Models and Performance Evaluation for 5G Millimeter-Wave Bands," in IEEE Transactions on Vehicular Technology, pp. 1-1, June 2018.

[8] J. K. N. Nyarko, C. A. Mbom, R. Yao and L. Wang, "Asymptotic Capacity of Rician Fading Channel for Large Scale Antenna Systems," AFRICON, 2015, Addis Ababa, 2015, pp. 1-5.

[9] C. T. Neil, M. Shafi, P. J. Smith, P. A. Dmochowski and J. Zhang, "Impact of Microwave and mmWave Channel Models on 5G Systems Performance," in IEEE Transactions on Antennas and Propagation, vol. 65, no. 12, pp. 6505-6520, Dec. 2017.

[10] T. L. Marzetta, "EM Algorithm for Estimating the Parameters of a Multivariate Complex Rician Density for Polarimetric SAR," Acoustics, Speech, and Signal Processing, 1995. ICASSP-95., 1995 International Conference on, Detroit, MI, 1995, pp. 3651-3654 vol.5.

[11] L. J. Greenstein, D. G. Michelson and V. Erceg, "Moment-Method Estimation of the Ricean K-Factor," in IEEE Communications Letters, vol. 3, no. 6, pp. 175-176, June 1999.

[12] K. E. Baddour and T. J. Willink, "Improved Estimation of the Ricean K-Factor from I/Q Fading Channel Samples," in IEEE Transactions on Wireless Communications, vol. 7, no. 12, pp. 5051-5057, December 2008.

[13] L. Lauwers, K. Barbe, W. Van Moer and R. Pintelon, "Estimating the Parameters of a Rice Distribution: A Bayesian Approach," Instrumentation and Measurement Technology Conference, 2009. I2MTC '09. IEEE, Singapore, 2009, pp. 114-117.

[14] T. S. Rappaport et al., "Millimeter Wave Mobile Communications for 5G Cellular: It Will Work!," in IEEE Access, vol. 1, no. , pp. 335-349, 2013.

[15] R. J. C. Bultitude and A. W. Leslie, "Propagation Measurement-Based Probability of Error Predictions for Digital Land Mobile Radio," IEEE Trans. Veh. Technol., Vol. 46, No.3, August, 1997, pp. 717-729.

[16] J. Zhang et al. "6-100 GHz research progress and challenges from a channel perspective for fifth generation (5G) and future wireless communication." Science China Information Sciences 60.8 (2017): 080301.

[17] J. Ko et al., "28 GHz Channel Measurements and Modeling in a Ski Resort Town in Pyeongchang for 5G Cellular Network Systems," 2016 10th European Conference on Antennas and Propagation (EuCAP), Davos, 2016, pp. 1-5.

[18] N. Sasaoka, Y. Adachi and Y. Itoh, "K Factor Estimation for MIMO Multipath Channels," 2015 IEEE International Conference on Digital Signal Processing (DSP), Singapore, 2015, pp. 1081-1084.

[19] H. Omote, Y. Ohta and T. Fujii, "Predicting the K-Factor of Divided Paths in Wideband Mobile Propagation," Vehicular Technology Conference, 2009. VTC Spring 2009. IEEE 69th, Barcelona, 2009, pp. 1-5.

[20] T. Zhou, C. Tao, L. Liu and Z. Tan, "Ricean K-Factor Measurements and Analysis for Wideband Radio Channels in High-Speed Railway U-Shape Cutting Scenarios," 2014 IEEE 79th Vehicular Technology Conference (VTC Spring), Seoul, 2014, pp. 1-5.

[21] M. K. Samimi, G. R. MacCartney, S. Sun and T. S. Rappaport, "28 GHz Millimeter-Wave Ultrawideband Small-Scale Fading Models in Wireless Channels," 2016 IEEE 83rd Vehicular Technology Conference (VTC Spring), Nanjing, 2016, pp. 1-6.

[22] S. Sun, et al. "Millimeter Wave Small-Scale Spatial Statistics in an Urban Microcell Scenario." arXiv preprint arXiv:1703.08239 (2017).

[23] S. Hur et al., "Proposal on Millimeter-Wave Channel Modeling for 5G Cellular System," in IEEE Journal of Selected Topics in Signal Processing, vol. 10, no. 3, pp. 454-469, April 2016.

[24] A. E. N. Liou, H. H. H. Huang and D. G. Michelson, "Issues in the Estimation of Ricean K-Factor from Correlated Samples," 2006 IEEE 64th Vehicular Technology Conference (VTC Fall), Montreal, 2006, pp. 1-4.

[25] C. Tepedelenlioglu, A. Abdi and G. B. Giannakis, "The Ricean K Factor: Estimation and Performance Analysis," in IEEE Transactions on Wireless Communications, vol. 2, no. 4, pp. 799-810, July 2003.

[26] R. J. C. Bultitude, "Estimating frequency correlation functions from propagation measurements on fading radio channels: a critical review," in IEEE Journal on Selected Areas in Communications, vol. 20, no. 6, pp. 1133-1143, Aug 2002.

[27] L. Bernadó et al., "Multi-dimensional K-factor analysis for V2V radio channels in open sub-urban street crossings," 21st Annual IEEE International Symposium on Personal, Indoor and Mobile Radio Communications, Instanbul, 2010, pp. 58-63.

[28] C. A. Gutierrez and M. Cabrera, "Issues of the Simulation of Wireless Channels with Exponential-Decay Power-Delay Profiles," 2005 IEEE 16th International Symposium on Personal, Indoor and Mobile Radio Communications, Berlin, 2005, pp. 507-511.

[29] W. C. Jakes, "Microwave Mobile Communications," Wiley-IEEE Press, 1994.

[30] X. Gao, L. Tian, P. Tang, T. Jiang, B. Liu and J. Zhang, "Channel Characteristics Analysis of Angle and Clustering in Indoor Office Environment at 28 GHz," Vehicular Technology Conference (VTC Fall), 2016 IEEE 84nd, Montreal, MA, 2016.

[31] X. Chen, L. Tian, P. Tang, T. Jiang and J. Zhang, "Modeling of Human Body Shadowing Based on 28 GHz Measurement Results," Vehicular Technology Conference (VTC Fall), 2016 IEEE 84nd, Montreal, MA, 2016. (A)

[32] F. J. Massey, "The Kolmogorov-Smirnov Test for Goodness of Fit," American Statistical Association Journal, March, 1951.

[33] H. W. Lilliefors, "On the Kolmogorov-Smirnov Test for the Exponential Distribution with Mean Unknown." Journal of the American Statistical Association 64.325 (1969): 387-389.

[34] R. A. Olea, and P. Vera, "Kolmogorov-Smirnov Test for Spatially Correlated Cata." Stochastic Environmental Research and Risk Assessment 23.6 (2009): 749-757.

[35] 3GPP, "Technical Specification Group Radio Access Network; Channel Model for Frequency Spectrum Above 6 GHz," TR 38.900, 3rd Generation Partnership Project (3GPP), June. 2016.

[36] R. J. C. Bultitude, "Measurement, Characterisation and Modelling of Indoor 800/900 MHz Radio Channels for Digital Communications," IEEE Communications Magazine, Vol. 25, No. 6, June 1987, pp. 5-12.

[37] A. F. Molisch, H. Asplund, R. Heddergott, M. Steinbauer and T. Zwick, "The COST259 Directional Channel Model-Part I: Overview and Methodology," in IEEE Transactions on Wireless Communications, vol. 5, no. 12, pp. 3421-3433, December 2006.

Pan Tang received the B.S. degree in electrical information engineering from the South China University of Technology, Guangzhou, China, in 2013 and completed two years of M.S. courses in the Beijing University of Posts and Telecommunications School of Information and Communication Engineering, Beijing, China in 2015, where he is currently working toward the Ph.D. degree in information and communication engineering. From 2017 to 2018, he was a Visiting Scholar with the University of Southern California. His current research interests include mmWave channel modelling, V2V channel modelling and signal estimation.

Jianhua Zhang received B.S. from the North China University of Technology in 1994 and Ph.D. degrees from the Beijing University of Posts and Telecommunications (BUPT) in 2003. Now she is the professor of information and engineering college, BUPT. She has published more than 70 journal papers and nearly 200 conference papers. She received China Communications Best Paper award at 2016 and shared VTC 2015 spring, JCN2009 best paper awards. She continuously contributed to channel model standards from ITU-R M.2135 to 3GPP 36.873,900/901 and she was the Drafting Group (DG) Chairwoman of ITU-R IMT-2020 channel model. Her research interests are massive MIMO and millimeter wave channel modeling and transmission techniques, channel emulator, OTA test and etc.

This article has been accepted for publication in a future issue of this journal, but has not been fully edited. Content may change prior to final publication. Citation information: DOI 10.1109/TVT.2018.2878352, IEEE Transactions on Vehicular Technology

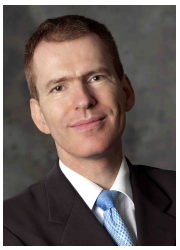

Andreas F. Molisch is the Solomon Golomb - Andrew and Erna Viterbi Chair Professor at the University of Southern California. He previously was at TU Vienna, AT&T (Bell) Labs, Lund University, and Mitsubishi Electric Research Labs. His research interest is wireless communications, with emphasis on wireless propagation channels, multi-antenna systems, ultrawideband signaling and localization, novel modulation methods, and caching for wireless content distribution. He is the author of four books, 19 book chapters, more than 220 journal papers, 300 conference papers, as well as 80 patents. He is a Fellow of the National Academy of Inventors, IEEE, AAAS, and IET, as well as Member of the Austrian Academy of Sciences and recipient of numerous awards.

Peter Smith received the B.Sc degree in Mathematics and the Ph.D degree in Statistics from the University of London, London, U.K., in 1983 and 1988, respectively. From 1983 to 1986 he was with the Telecommunications Laboratories at GEC Hirst Research Centre. From 1988 to 2001 he was a lecturer in statistics at Victoria University of Wellington, New Zealand. From 2001 to 2015 he worked in Electrical and Computer Engineering at the University of Canterbury. In 2015 he joined Victoria University of Wellington as Professor of Statistics. His research interests include the statistical aspects of design, modeling and analysis for communication systems, especially antenna arrays, MIMO, cognitive radio, massive MIMO and mmWave systems.

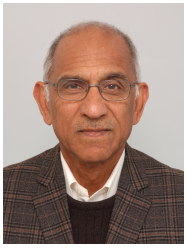

Mansoor Shafi received the B.S. and Ph.D. degrees in electrical engineering from the University of Engineering and Technology at Lahore and the University of Auckland in 1970 and 1979, respectively. He is currently employed with Spark NZ and is a Telecom Fellow and an Adjunct Professor with the School of Engineering, Victoria University. He has authored over 150 journal papers in wireless communications. He has co-shared Best Tutorial Paper Award from the IEEE Communications Society in 2004 and the IEEE Donald G. Fink Award 2011. He was awarded member of the New Zealand Order of Merit in the Queens Birthday Honors 2013 for services to wireless communications.

Lei Tian received the B.S. degree in Communication Engineering and Ph.D degree in Information and Communication Systems from Beijing University of Posts and Telecommunications (BUPT) in 2009 and 2015, respectively. He has been dedicated to the research on wireless channel measurement and modeling, including wireless wideband channel measurement method, MIMO channel measurement method, channel parameter estimation, modeling of large-scale and small-scale channel characteristics, and wireless channel modeling. Recently, He mainly focuses on the channel measurement and modeling of mmWave and massive MIMO for 5G mobile communication system.